Diffuse laser cooling based on the $6P_{3/2}$ excited state of rubidium atoms via 420 nm blue light

Jia Zhang,[1] Xun Gao,[1] Zheng Xiao,[1] Xiaolei Guan,[1] Ruihang Chen,[1] Mengyuan Han,[1] Tiantian Shi,[2,3,*] and Jingbiao Chen[1,2,4]

[1]*Institute of Quantum Electronics, School of Electronics, Peking University, Beijing 100871, China*

[2]*National Key Laboratory of Advanced Micro and Nano Manufacture Technology, School of Integrated Circuits, Peking University, Beijing 100871, China*

[3]*Beijing Advanced Innovation Center for Integrated Circuits, Beijing 100871, China*

[4]*Hefei National Laboratory, Hefei 230088, China*

(Received 24 September 2025; accepted 18 August 2026; published 10 September 2026)

To date, the laser cooling of rubidium atoms has inevitably relied on 780 nm cooling light corresponding to the first excited state $5P_{3/2}$. Here, we demonstrate diffuse laser cooling of ^{87}Rb atoms using the 420 nm $5S_{1/2} \rightarrow 6P_{3/2}$ transition without a preceding 780 nm cooling stage. A high-power 420 nm laser is used as the cooling light to produce cold atoms in a 1-m-long diffuse-cooling cell. Absorption spectroscopy yields a cold-atom density of approximately 1.4×10^{11} m^{-3}. We compare the cooling performance of the 420 nm and conventional 780 nm diffuse-cooling schemes and verify the feasibility of using the high-excited-state transition as an independent cooling channel in this large-volume diffuse-cooling system. This approach provides an alternative cooling/pumping pathway for continuous cold-atom active optical clocks, where compatibility with the clock-lasing process and reduced cooling-light-induced perturbations are important. It is also expected to open up research directions and application prospects in frontier fields such as Rydberg atoms, quantum information, and so on.

DOI: 10.1103/4jtk-471b

I. INTRODUCTION

The disorder induced by the atomic thermal motion has long been one of the major obstacles hindering in-depth exploration of internal quantum states [1] and their interactions, precise measurement of fundamental physical constants [2], and even the realization of quantum precision manipulation [3,4]. Slowing down and cooling atoms to extremely low temperatures to render them nearly "stationary" is the key to overcoming these obstacles and opening up new frontiers in modern atomic and molecular physics as well as quantum technology. Laser cooling technology achieves efficient deceleration and cooling of free atoms through momentum exchange between photons and atoms [5–7], and its emergence and development undoubtedly represent a revolutionary breakthrough. Precise manipulation of atomic motion to near-stationary ultracold states serves as a core methodology in modern atomic and molecular physics [8,9], quantum precision measurement [10–13], and quantum information science [14,15].

Among numerous atomic systems, rubidium atoms have become one of the most widely used platforms in cold-atom research, owing to their mature laser technology (D2 line $5S_{1/2}$–$5P_{3/2}$ with a wavelength of 780 nm [16]) and favorable energy level characteristics (electric dipole-allowed strong transitions and closed cycle transitions). Cooling technologies based on 780 nm lasers, such as Doppler cooling [17,18], polarization gradient cooling [19], Raman sideband cooling [20–22], and magneto-optical trap [23,24], have reached a high level of maturity. They can efficiently cool and trap large numbers of rubidium atoms to the Doppler-cooling temperature limit or even sub-Doppler temperatures, laying the foundation for numerous cutting-edge research fields, including Bose-Einstein condensation [20], atomic clocks [25], and atomic interferometers [26]. In relevant studies on laser cooling of rubidium atoms, most systems employ cooling and repumping light addressing different hyperfine sublevels within the same set of fine-structure energy levels. However, the frequencies of the pumping and cooling light predominantly concentrate on red transitions near 780 and 795 nm in rubidium, while research on blue-light cooling corresponding to the 420 and 421 nm transitions of the high excited state remains relatively scarce.

Conventional 780 nm cooling schemes possess a relatively large natural linewidth ($\Gamma_{780}/2\pi = 6.06$ MHz [16,27]). While this facilitates high photon-scattering rates for rapid initial cooling, it also imposes a relatively high Doppler-cooling temperature limit. Furthermore, the comparatively short lifetime of the $5P_{3/2}$ level imposes constraints on further advancing coherent manipulation. Current research utilizing the $6P_{3/2}$ excited state of rubidium atoms as the cooling level consistently integrates both 780 and 420 nm cooling [28,29].

*Contact author: tts@pku.edu.cn

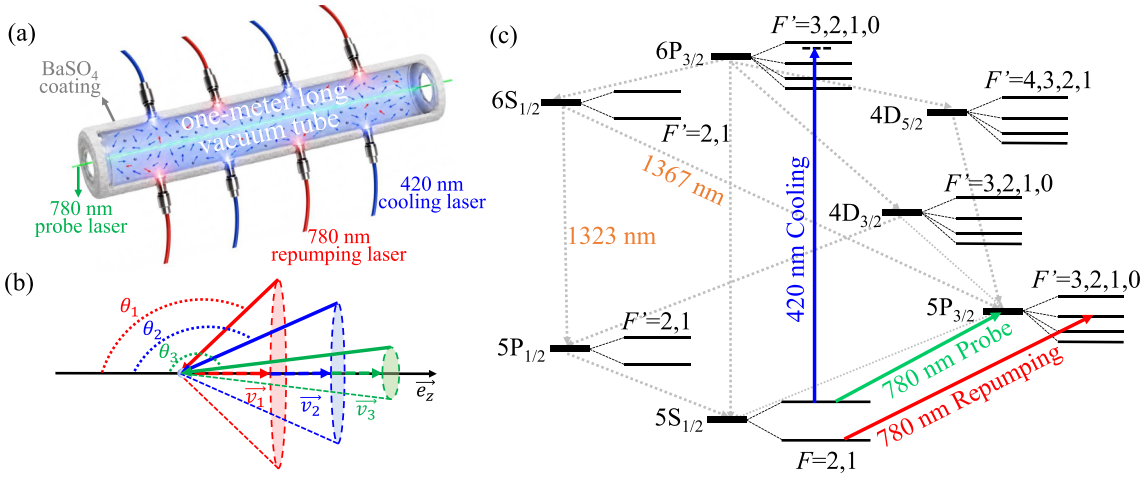

FIG. 1. (a) Schematic of 420 nm diffuse laser cooling of rubidium atoms in a meter-scale vacuum glass tube. (b) The Doppler resonance condition within the quasi-isotropic diffuse light field. (c) Relevant energy levels involved in the 420 nm cooling scheme. The cooling light is red detuned from the 420 nm $5S_{1/2}(F = 2) \rightarrow 6P_{3/2}(F' = 3)$ transition. The repumping light addresses the 780 nm $5S_{1/2}(F = 1) \rightarrow 5P_{3/2}(F' = 2)$ transition, while the probe light is near the 780 nm $5S_{1/2}(F = 2) \rightarrow 5P_{3/2}$ transition. The 420 nm cooling light also serves as the pumping light for the active-clock transition by populating the $6P_{3/2}$ state, from which cascade decay can establish population inversion between $6S_{1/2}$ and $5P_{3/2}$ or $5P_{1/2}$, corresponding to the 1367 and 1323 nm lasing transitions.

The first approach involves preliminary cooling with 780 nm lasers, followed by secondary cooling using 420 nm blue light [28]. In essence, it utilizes the broad linewidth of 780 nm (∼6.06 MHz) to achieve efficient trapping and initial deceleration, and then leverages the narrow linewidth of 420 nm blue light ($\Gamma_{420}/2\pi = 1.42$ MHz) [30,31] to break through the temperature limit of 780 nm laser cooling. This process necessitates laser source switching and critically depends on the preliminary cooling stage. Another approach is the dual-light cooperative cooling scheme [29]: Both 780 and 420 nm lasers are turned on simultaneously, but the 780 nm light still serves as the dominant cooling light, with the 420 nm light playing an auxiliary role. This configuration retains a fundamental reliance on the 780 nm light source and introduces complexities associated with spectral interference and power-matching requirements.

In this work, we demonstrate independent 420 nm laser cooling on the $5S_{1/2} \rightarrow 6P_{3/2}$ transition using a diffuse laser cooling configuration [32–35]. By employing a highly reflective barium sulfate ($BaSO_4$) coating to multiply scatter the cooling light, we generate a quasi-isotropic light field that enables large-volume cooling without complex optical alignments or magnetic fields. Unlike previous schemes that require a 780 nm precooling stage, we directly utilize the 420 nm $5S_{1/2} \rightarrow 6P_{3/2}$ high-excited-state transition as the cooling transition within this diffuse light field. Our goal is not to replace conventional 780 nm cooling, but to verify this high-excited-state transition as a stand-alone cooling channel. Experimentally, we produce cold ^{87}Rb atoms in a 1-m-long diffuse-cooling cell, detect them via axial 780 nm absorption spectroscopy, and compare the cooling performance with that of conventional 780 nm diffuse cooling. This single-stage 420 nm cooling scheme is primarily motivated by continuous cold-atom active optical clocks [36,37], where the 420 nm laser simultaneously cools and pumps atoms without perturbing the clock-lasing process. Furthermore, it opens new avenues for Rydberg atom preparation [38], 420 nm optical frequency standards [39–41], and atom interferometry [42].

II. THEORETICAL CONSIDERATIONS

As shown in Fig. 1(a), the diffuse-cooling geometry consists of a 1-m-long glass tube coated with barium sulfate ($BaSO_4$), which creates a quasi-isotropic light field through multiple reflections of the injected laser beams. Following the isotropic-light-cooling model of Ref. [43], the ideal diffuse field is treated as a continuous distribution of plane-wave components over all propagation directions. In the low-saturation, two-level approximation, the mean radiation-pressure force on an atom with velocity $\mathbf{v}$ is

$$\mathbf{F}_{\rm iso}(\mathbf{v}) = \frac{\hbar k \Gamma}{2} \int_{4\pi} \frac{\tilde{s}_0 \mathbf{n}}{1 + 4(\delta - k\mathbf{n}\cdot\mathbf{v})^2/\Gamma^2}\, d\Omega, \qquad (1)$$

where $\hbar$, Γ, k, δ, and $\mathbf{n}$ denote the reduced Planck constant, natural linewidth in angular-frequency units, wave number, laser detuning, and propagation-direction unit vector, respectively. For an isotropic field, $\tilde{s}_0 = S_{\rm iso}/(4\pi)$ is the on-resonance saturation parameter per unit solid angle, with $S_{\rm iso}$ denoting the global saturation parameter of the isotropic field. Rotational symmetry eliminates the force components transverse to $\mathbf{v}$, giving zero net force for a stationary atom and a damping force opposite to $\mathbf{v}$ for a moving atom under red-detuned illumination.

As illustrated in Fig. 1(b), the resonance condition $\delta = kv\cos\theta$ defines a velocity-dependent cone of resonant propagation directions, where θ is the angle between $\mathbf{n}$ and $\mathbf{v}$. For red detuning ($\delta < 0$), the resonant components satisfy $\cos\theta < 0$ and therefore propagate predominantly opposite to the atomic motion. Different velocity classes consequently interact with different angular components of the diffuse field, providing a three-dimensional Doppler-cooling force.

The atomic transitions involved in diffuse laser cooling are shown in Fig. 1(c), and the relevant parameters of

TABLE I. Comparison between 780 nm Doppler cooling and 420 nm Doppler cooling.

λ (nm)	Corresponding energy levels	$\Gamma/2\pi$ (MHz)	T_D (μK)	v_p (m/s)
780	$5S_{1/2} \rightarrow 5P_{3/2}$	6.06 [16,27]	146	0.167
420	$5S_{1/2} \rightarrow 6P_{3/2}$	1.42 [30,31]	34	0.081

the 780 and 420 nm cooling transitions are summarized in Table I. Here, $T_D = \hbar\Gamma/(2k_B)$ is the Doppler temperature of an ideal two-level atom, and $v_p = \sqrt{2k_B T_D/m}$ is the corresponding most probable thermal speed, with k_B and m denoting the Boltzmann constant and atomic mass, respectively. The narrower linewidth of the 420 nm transition yields a lower Doppler-temperature scale but also a smaller velocity-capture range and photon-scattering rate than the conventional 780 nm transition. In addition, cascade decay from the $6P_{3/2}$ state through the $6S_{1/2}$, $4D_{3/2}$, and $4D_{5/2}$ states makes the cooling cycle open. These properties motivate the use of relatively large red detuning and high optical intensity for direct 420 nm cooling.

III. EXPERIMENT

The experimental optical layout and relevant partial energy levels are shown in Figs. 2(a) and 2(b), respectively. Because acousto-optic modulators (AOMs) at 420 nm have relatively low diffraction efficiency, shifting the high-power cooling beam after frequency locking would introduce substantial optical loss. We therefore apply the frequency shift in the spectroscopy branch before locking. Since $\Gamma_{420}/2\pi = 1.42$ MHz and the required red detuning is only several megahertz, two AOMs operated in the +1st and −1st diffraction orders are used to produce a small net positive frequency offset. The frequency-shifted beam is then locked to the ^{87}Rb $5S_{1/2}(F = 2) \rightarrow 6P_{3/2}(F' = 3)$ transition using modulation-transfer spectroscopy, leaving the unshifted cooling beam stably red detuned from resonance while avoiding AOM-induced power loss. The open decay channels from the $6P_{3/2}$ state through the $4D_{3/2}$, $4D_{5/2}$, and $6S_{1/2}$ states can transfer atoms to the dark $5S_{1/2}(F = 1)$ ground state. A 780 nm laser is therefore locked to the $5S_{1/2}(F = 1) \rightarrow 5P_{3/2}(F' = 2)$ transition using saturated-absorption spectroscopy and employed as the repumping light. Rate-equation calculations indicate that, without repumping, atoms rapidly accumulate in the $5S_{1/2}(F = 1)$ state and the cooling cycle is effectively quenched.

The core of our vacuum and cooling apparatus is illustrated in the three-dimensional schematic of Fig. 2(c). It consists of a cylindrical vacuum atomic cell fabricated from glass, with a length of 1 m and a diameter of 2 cm. The vacuum environment is maintained by an ion pump with a pumping speed of 45 l/s, achieving a background vacuum level on the order of 10^{-6} Pa. To explicitly address the atomic supply mechanism, the rubidium vapor is provided by a reservoir-type source attached to the vacuum system, as marked in Fig. 2(c). This source contains a natural isotopic mixture (approximately 72% ^{85}Rb and 28% ^{87}Rb) initially sealed in a glass ampoule

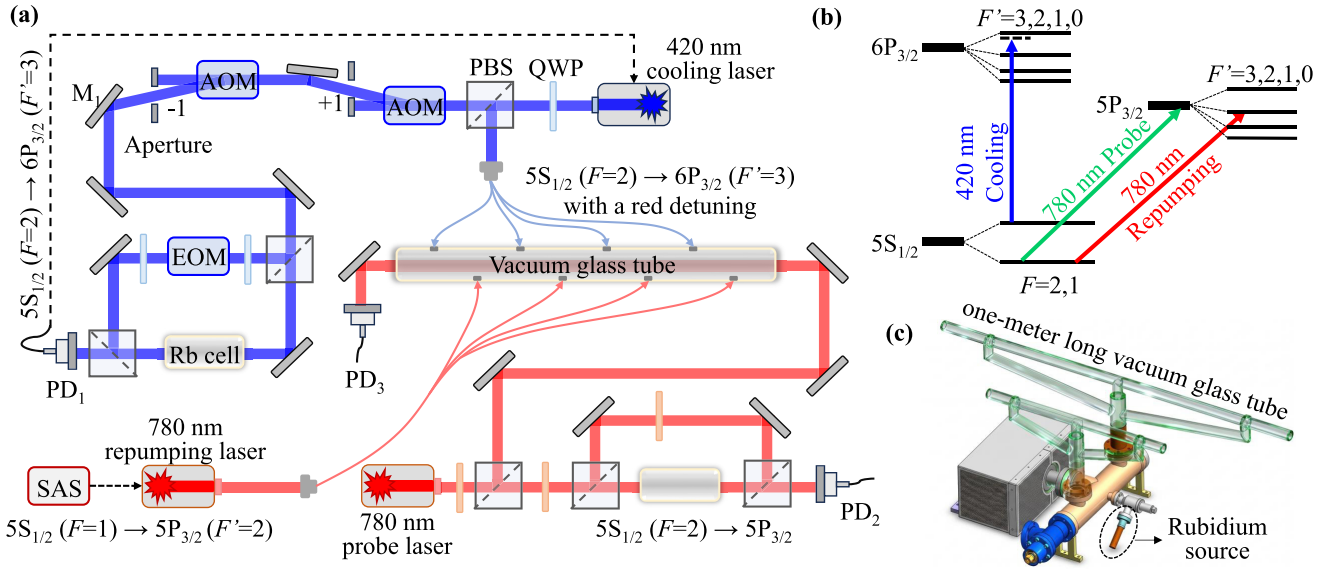

FIG. 2. Experimental system. (a) The 420 nm laser undergoes frequency shifting before frequency locking, resulting in a 420 nm cooling light with a specific red detuning relative to the $5S_{1/2}(F = 2) \rightarrow 6P_{3/2}(F' = 3)$ transition. The 780 nm repumping light is locked to the $5S_{1/2}(F = 1) \rightarrow 5P_{3/2}(F' = 2)$ transition, while the probe light corresponds to the 780 nm $5S_{1/2}(F = 2) \rightarrow 5P_{3/2}$ transition. (b) Relevant energy levels. (c) Schematic illustration of the overall vacuum system apparatus, explicitly highlighting the 1-m-long vacuum glass tube coated with $BaSO_4$ and the reservoir-type rubidium source.

within a crushable copper tube. Upon establishing the background vacuum, the copper tube is mechanically crushed from the outside to break the glass ampoule and release the atoms. The rubidium vapor subsequently diffuses along the 1-m cell until reaching adsorption saturation on the inner walls. At an ambient room temperature of 22 °C, the system achieves thermal equilibrium, yielding a steady rubidium vapor pressure of approximately 2×10^{-7} Pa governed by the cell wall temperature.

To generate the diffuse laser cooling light field, a $BaSO_4$ diffuse reflection coating is uniformly applied to the outer wall of the vacuum cell. This coating possesses a high reflectivity of approximately 95% for the 420 nm laser and 98% for the 780 nm laser. The 420 nm cooling light and 780 nm repumping light are coupled into multimode fibers and injected into this diffuse-coated cell. Within the cell, the generated diffuse light field exhibits quasi-isotropic intensity and frequency distributions [32–35]. To interrogate the resulting cold ^{87}Rb ensemble, a homemade 780 nm interference-filter external-cavity diode laser [44] is employed as the probe beam, which propagates axially along the 1-m-long vacuum cell.

IV. RESULTS

A. Absorption spectroscopy of cold ^{87}Rb atoms

The 420 nm cooling light is red detuned by approximately 8 MHz from the ^{87}Rb $5S_{1/2}(F = 2) \rightarrow 6P_{3/2}(F' = 3)$ transition, while a 30 mW repumping laser is resonant with the $5S_{1/2}(F = 1) \rightarrow 5P_{3/2}(F' = 2)$ transition. Under these conditions, the diffuse light field decelerates and cools the atoms within the 1-m-long cell, as shown in Fig. 3(a). The cooled atoms are detected using a weak axial 780 nm probe with microwatt-level power, whose frequency is scanned across the three allowed D2 transitions from $5S_{1/2}(F = 2)$ to $5P_{3/2}(F' = 1, 2, 3)$. Because the 420 nm cooling scheme produces fewer cold atoms than conventional 780 nm cooling, a narrow cold-atom absorption feature is clearly resolved against the broad thermal background only at the $F = 2 \rightarrow F' = 3$ transition, as shown by the blue curve in Fig. 3(b). The narrow feature arises from the cold-atom fraction (∼0.7%), whereas the broad background is dominated by the thermal population.

Because conventional time-of-flight thermometry is not applicable to the present geometry, the cold-atom absorption linewidth is used to estimate a conservative upper temperature bound. Using a simultaneously recorded rubidium saturated-absorption spectrum as the frequency reference, the absorption feature obtained under 420 nm cooling is fitted with a Voigt profile, as shown in Fig. 3(c), yielding a Gaussian linewidth of $\Delta\nu_G = 1.56$ MHz. If this Gaussian contribution is entirely attributed to Doppler broadening, $T = \frac{m\lambda^2(\Delta\nu_G)^2}{8k_B \ln 2}$ gives an upper bound of 2.81 mK, where λ is the probe wavelength. Because unresolved nonthermal broadening may also contribute to $\Delta\nu_G$, this value should not be interpreted as the actual cold-atom temperature.

For comparison, conventional 780 nm diffuse cooling was implemented in the same cell. The cooling light was red detuned by approximately 15 MHz from the ^{87}Rb $5S_{1/2}(F = 2) \rightarrow 5P_{3/2}(F' = 3)$ transition, while the repumping light remained resonant with the $5S_{1/2}(F = 1) \rightarrow 5P_{3/2}(F' = 2)$ transition. The resulting cold-atom spectrum was measured using the same axial probe. By precisely controlling the frequency and intensity of both the cooling and repump lights, a significantly improved cooling effect for ^{87}Rb atoms is ultimately achieved. After the rubidium atoms are cooled, a 780 nm probe beam is similarly used to detect the cold atomic cloud.

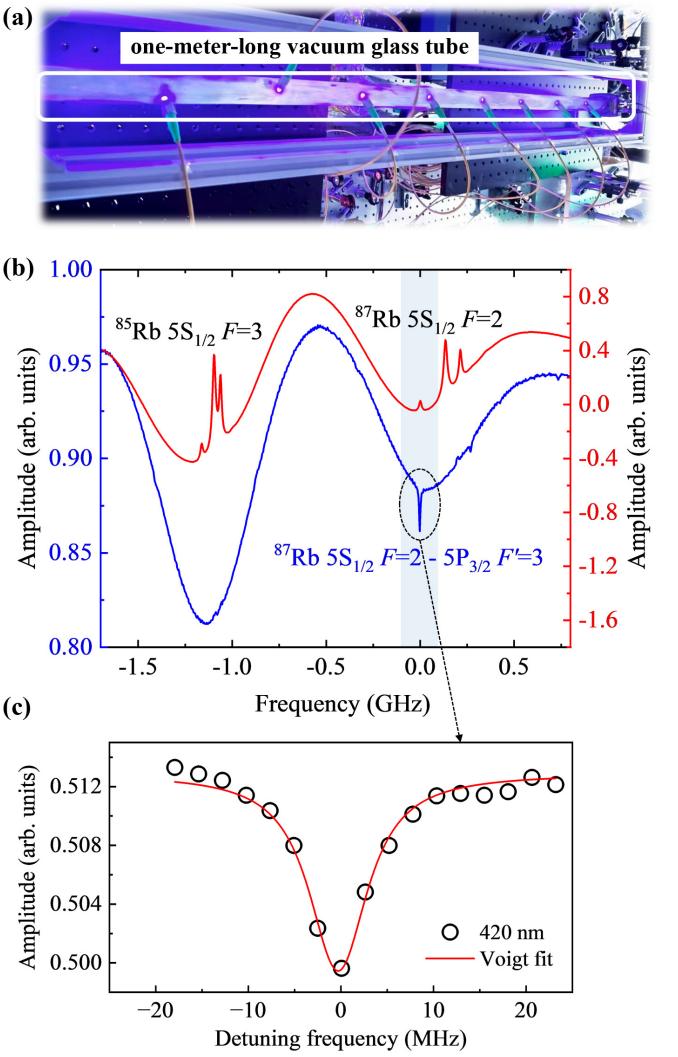

FIG. 3. (a) Under the cooling effect of the 420 nm diffuse light field, diffuse cooling is implemented throughout the 1-m-long cell, and the cold-atom absorption is probed along the axial direction. (b) Absorption spectroscopy of cold ^{87}Rb atoms for the 780 nm probe light (blue curve). The red curve serves as the reference rubidium saturated-absorption spectroscopy. Cold atomic absorption can be observed at the position corresponding to the ^{87}Rb $5S_{1/2}(F = 2) \rightarrow 5P_{3/2}(F' = 3)$ transition. (c) Voigt fit to the cold-atom absorption feature obtained under 420 nm cooling.

The resulting cold-atom absorption spectroscopy is shown in Figs. 4(a) and 4(b). Due to the higher efficiency of 780 nm laser cooling, the number of cold atoms obtained is substantially increased. Consequently, three absorption peaks are visible, corresponding to the transitions $5S_{1/2}(F = 2) \rightarrow 5P_{3/2}(F' = 1, 2, 3)$, respectively. The corresponding Voigt fit for the 780 nm cooling scheme is shown in Fig. 4(c). The

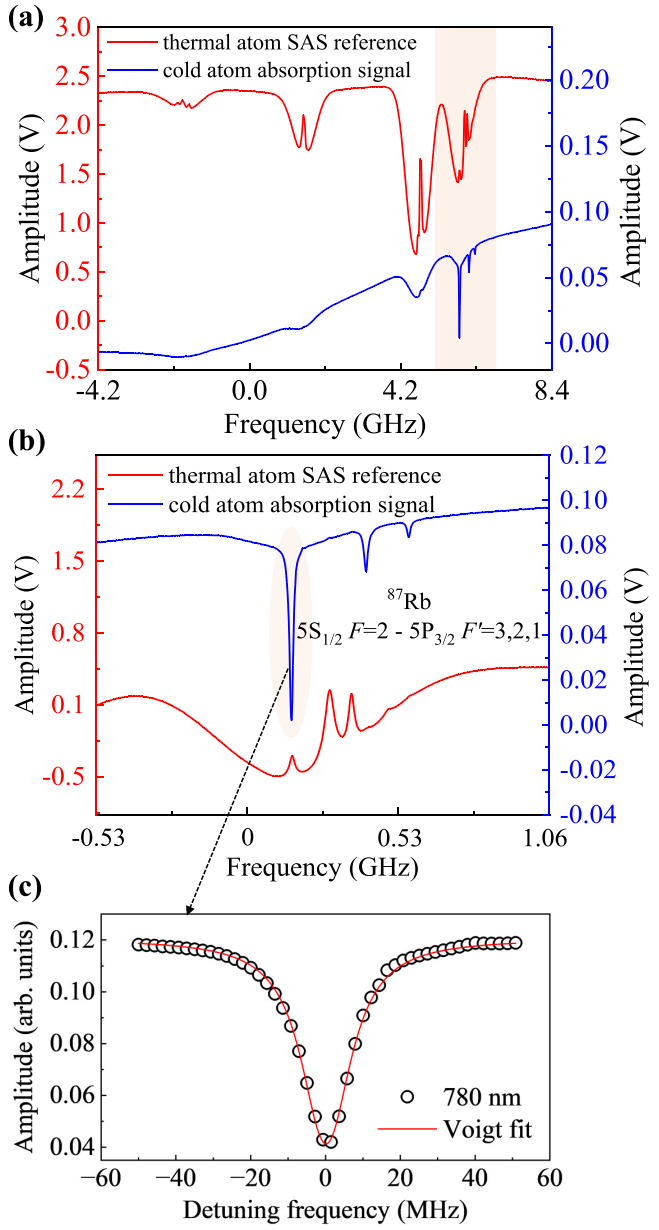

FIG. 4. Absorption spectrum of cold ^{87}Rb atoms obtained under conventional 780 nm diffuse laser cooling. (a) Full absorption spectrum containing the relevant transitions of ^{85}Rb and ^{87}Rb. (b) Expanded spectrum showing the resolved ^{87}Rb $5S_{1/2}(F = 2) \rightarrow 5P_{3/2}(F' = 1, 2, 3)$ cold-atom absorption features. (c) Voigt fit to the cold-atom absorption feature under 780 nm cooling.

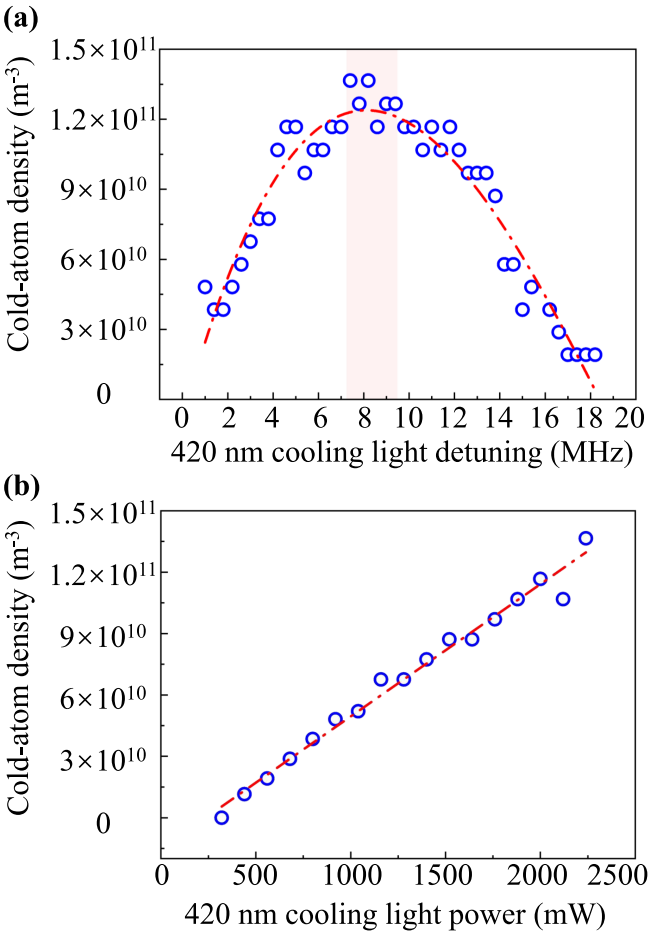

FIG. 5. Cold-atom density within the 780 nm probed region under 420 nm diffuse laser cooling. (a) Dependence on the red detuning of the 420 nm cooling light from the ^{87}Rb $5S_{1/2}(F = 2) \rightarrow 6P_{3/2}(F' = 3)$ transition. The maximum is obtained at a detuning of approximately 8 MHz. (b) Dependence on the injected 420 nm cooling-light power at the optimal detuning. No saturation is observed over the investigated power range of 0–2.5 W. The red dashed curves are empirical fits to the experimental data. The shaded region indicates the favorable detuning range around the maximum cold-atom density.

extracted Gaussian linewidth is 1.66 MHz, giving a conservative upper temperature bound of 3.16 mK under the same assumption. As in the 420 nm case, this value contains unresolved nonthermal broadening and therefore represents only a loose constraint on the actual cloud temperature. Moreover, the microscopically inhomogeneous polarization distribution produced by multiple diffuse reflections can support sub-Doppler polarization-gradient cooling [45–48], suggesting that the actual atomic temperature may be substantially lower than this spectroscopy-based upper bound.

B. Optimization of the cooling-light parameters

The absorption of the weak 780 nm probe is used to determine the probe-volume-averaged cold-atom density and optimize the 420 nm cooling parameters. Figure 5(a) shows the cold-atom density as the red detuning of the 420 nm cooling light from the ^{87}Rb $5S_{1/2}(F = 2) \rightarrow 6P_{3/2}(F' = 3)$ transition is varied from 0 to 18 MHz. The cold-atom density presents an increasing and then a decreasing trend with increasing detuning, reaching its maximum at approximately 8 MHz. At smaller detunings, strong near-resonant photon scattering increases recoil heating and reduces the cold-atom density. At larger detunings, the reduced photon-scattering rate weakens the cooling force. The optimum near 8 MHz therefore reflects a balance among scattering strength, recoil heating, and velocity capture.

Cooling-light power is another important optimization parameter. After frequency shifting, frequency locking, and multimode-fiber coupling, the 3 W 420 nm laser provides a maximum power of approximately 2.5 W at the entrance of the vacuum cell. Figure 5(b) shows the probe-volume-averaged cold-atom density as the injected cooling-light power is varied from 0 to 2.5 W. The cold-atom density increases monotonically with cooling-light power, with no plateau observed over the investigated range. At an injected power of 2.5 W, the probe-volume-averaged cold-atom density reaches approximately 1.4×10^{11} m^{-3}.

To determine this probe-volume-averaged density quantitatively, the absorption of the weak axial 780 nm probe is analyzed using the Beer-Lambert law [49]. The optical depth is given by $\mathrm{OD} = -\ln\left(\frac{I_{\mathrm{trans}} - I_{\mathrm{dark}}}{I_0 - I_{\mathrm{dark}}}\right)$, where I_0, I_{trans}, and I_{dark} are the incident probe intensity, transmitted probe intensity, and dark-field intensity arising from ambient light and the detector dark current, respectively. The probe power is maintained at the microwatt level to minimize probe-induced heating and absorption saturation. In addition, the broad absorption background arising from thermal atoms is subtracted before evaluating the cold-atom contribution. Using the resonant cross-section $\sigma_0 = \frac{3\lambda^2}{2\pi}$ for the 780 nm probe transition, the probe-volume-averaged cold-atom density is calculated as $\bar{n}_{\mathrm{p}} = \frac{\mathrm{OD}}{\sigma_0 L}$, where $L = 1$ m is the effective interaction length. Because the radial density distribution of the cold atomic cloud cannot be resolved in the present experimental geometry, the measured density is not extrapolated to the full volume of the cylindrical cell.

The measured $1/e^2$ intensity diameter of the probe beam is 1.2 mm, corresponding to a waist of $w_{\mathrm{p}} = 0.60$ mm. For the Gaussian probe mode, the effective transverse area is $A_{\mathrm{eff}} = \frac{\pi w_{\mathrm{p}}^2}{2}$, giving an effective probe volume of $V_{\mathrm{eff}} = A_{\mathrm{eff}} L = 5.65 \times 10^{-7}$ m^3. The effective cold-atom number sampled by the probe is therefore defined as $N_{\mathrm{eff}} = \bar{n}_{\mathrm{p}} V_{\mathrm{eff}}$. At an injected 420 nm cooling power of 2.5 W, the maximum density reported above corresponds to an effective atom number of approximately 7.9×10^4 sampled in the probed region.

In the diffuse light field, photons undergo multiple reflections, and the intracell energy density can be approximated as spatially uniform. The system can therefore be treated approximately as an integrating sphere, for which the intracell light intensity is estimated as $I_{\mathrm{in}} \approx \frac{P_{\mathrm{in}}}{A_{\mathrm{wall}}(1 - R_{\mathrm{eff}})}$, where P_{in} is the injected optical power, A_{wall} is the total internal surface area of the vacuum cell, and R_{eff} is the effective reflectivity. The reflectivity of the coating at 420 nm is approximately 95%. To approximately account for losses at the light-entry ports and the ends of the cell, an effective reflectivity of $R_{\mathrm{eff}} \approx 92\%$ is used. At an injected cooling-light power of 2.5 W, the intracell intensity is estimated to be approximately 49.3 mW/cm^2. This value corresponds to approximately 2.1 times the experimentally measured saturation intensity $I_{\mathrm{s},420} = (23.18 \pm 0.28)$ mW/cm^2 reported in Ref. [50], which is consistent with the theoretical value of 23.45 mW/cm^2.

The observed increase in the cold-atom density can be attributed to the higher diffuse-field intensity, which enhances the photon-scattering rate and improves the capture and cooling of the atoms. Although the estimated average intensity exceeds the saturation intensity, no saturation of the measured cold-atom density is observed. This indicates that the ensemble cooling performance is not determined solely by the saturation of the optical transition, but is also influenced by the spatial distribution of the diffuse field, the velocity-capture range, and the open multilevel decay dynamics. Further increases in cooling-light power may therefore enhance the cold-atom density.

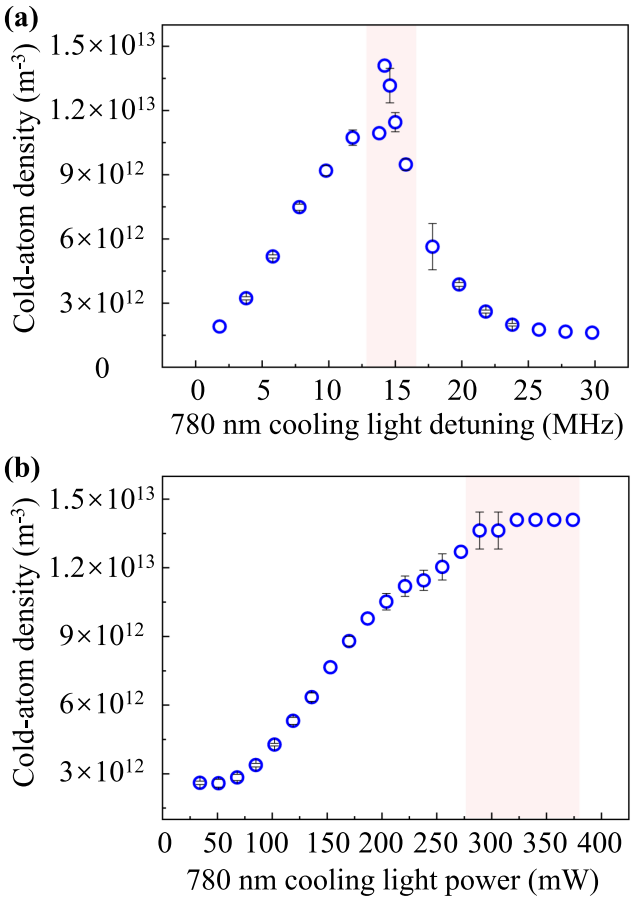

FIG. 6. Cold-atom density within the 780 nm probed region under 780 nm diffuse laser cooling. (a) Dependence on the red detuning of the cooling light from the ^{87}Rb $5S_{1/2}(F = 2) \rightarrow 5P_{3/2}(F' = 3)$ transition. The maximum is obtained at a detuning of approximately 15 MHz. (b) Dependence on the injected 780 nm cooling-light power at the optimal detuning. The shaded regions indicate the favorable operating ranges, corresponding to the vicinity of the optimal detuning in panel (a) and the near-saturation power regime in panel (b).

For comparison, conventional 780 nm diffuse cooling was also investigated. At an injected cooling-light power of 300 mW, the cold-atom density reaches its maximum at a red detuning of 15 MHz and decreases at larger detunings, as shown in Fig. 6(a). This optimal detuning corresponds to approximately 2.5 times the natural linewidth. At this detuning, the cold-atom density initially increases with cooling-light power, reaches a maximum near 300 mW, and then decreases slightly at higher powers, possibly because of recoil heating and saturation-induced imbalance, as shown in Fig. 6(b). For the ^{87}Rb $5S_{1/2}(F = 2) \rightarrow 5P_{3/2}(F' = 3)$ transition, the saturation intensity is $I_{\mathrm{s},780} = 1.67$ mW/cm^2. The

effective diffuse-field intensity at 300 mW is estimated to be 9.6 mW/cm^2, corresponding to approximately $5.7I_{s,780}$.

Under these optimal conditions, the cold-atom density is approximately 1.3×10^{13} m^{-3}, corresponding to an effective atom number of approximately 7.4×10^6 within the probed region. For reference, if the probe-volume-averaged densities are assumed to be spatially uniform throughout the entire cell, they would correspond to extrapolated total atom numbers of approximately 4.4×10^7 and 4.2×10^9 for the 420 and 780 nm cooling schemes, respectively. However, cold-atom clouds produced in isotropic cooling geometries are expected to exhibit an approximately Gaussian spatial distribution, with the density decreasing toward the reflecting surfaces [51]. Therefore, the total atom numbers inferred under the uniform-density assumption should be regarded only as rough order-of-magnitude estimates and may be overestimated.

V. DISCUSSION

The optimal detuning and saturation behavior of the 420 nm diffuse laser cooling differ significantly from the conventional 780 nm scheme. This distinct cooling dynamics stems fundamentally from the intrinsic properties of the blue transition. First, the momentum of a 420 nm photon is approximately 1.86 times that of a 780 nm photon ($p = \hbar k$). Consequently, each spontaneous emission cycle imparts a substantially larger recoil kick, making the fundamental recoil heating energy ($\propto k^2$) nearly 3.5 times higher. Second, the 420 nm transition features a much narrower natural linewidth and a larger wave number, resulting in an inherently narrow velocity-capture range ($v_c \propto \Gamma/k$). To effectively capture room-temperature thermal atoms and counteract the heightened recoil disturbance, it is necessary to employ a large red detuning and high optical power. Despite these stringent intrinsic physical constraints, the 420 nm diffuse light field successfully establishes a steady-state cold atomic cloud. This confirms that the high-excited-state transition can independently and effectively sustain cooling performance in a large-volume macroscopic diffuse field. The meter-scale cold atomic cloud can provide an extended interaction length and a large effective gain volume, which are beneficial for future active optical clock experiments.

While conventional 780 nm cooling remains the superior technique for preparing large-number atomic ensembles, the independent 420 nm cooling channel circumvents the severe limitations of 780 nm light in continuous four-level cold-Rb-atom active optical clocks. Continuous operation requires simultaneous cooling and lasing. However, introducing 780 nm cooling light ($5S_{1/2} \rightarrow 5P_{3/2}$) induces a massive ac Stark shift that destroys clock coherence: It directly addresses the lower level of the 1367 nm clock transition and creates extreme near-resonant crosstalk for the 1323 nm clock transition. This fatal physical interference forces traditional systems into a pulsed operation mode.

In contrast, the 420 nm scheme ($5S_{1/2} \rightarrow 6P_{3/2}$) is detuned from the clock transitions by hundreds of nanometers, inherently minimizing light-shift perturbations. Furthermore, it provides an integrated cooling and pumping mechanism: The 420 nm laser simultaneously cools the atoms and excites them to the $6P_{3/2}$ state, establishing the required population inversion through cascade decay. This eliminates the need for separate pumping sources, offering a compact and robust route for continuous active optical clocks.

VI. CONCLUSION

In summary, we have experimentally demonstrated diffuse laser cooling of ^{87}Rb atoms using the 420 nm $5S_{1/2} \rightarrow 6P_{3/2}$ transition without a preceding 780 nm cooling stage. In the present large-volume diffuse-cooling configuration, this higher-excited-state transition serves as an independent cooling channel. At an injected cooling-light power of 2.5 W and an optimal red detuning of approximately 8 MHz, the probe-volume-averaged cold-atom density reaches approximately 1.4×10^{11} m^{-3}, corresponding to an effective atom number of approximately 7.9×10^4 sampled by the probed region. The main implication of this work is that ground-state rubidium atoms can be directly cooled by 420 nm blue light while being simultaneously excited to the $6P_{3/2}$ state. This method bypasses the conventional cooling route based on the first excited state of rubidium and the sequential path of 780 nm cooling followed by 420 nm cooling. It therefore provides an alternative technical route for combining laser cooling with high-excited-state preparation. This capability is particularly relevant to cold-atom active optical clocks, where simultaneous cooling and pumping are required for continuous operation. It may also be useful for future studies involving Rydberg-state preparation, blue-transition optical frequency standards, atom interferometry with blue transitions, and quantum manipulation based on highly excited atomic levels.

ACKNOWLEDGMENTS

This work was funded by National Natural Science Foundation of China (Grants No. 624B2010 and No. 62405007), the Innovation Program for Quantum Science and Technology 2021ZD0303200, and JSJL2024205XXXX.

J.C. conceived the idea to directly use a 420 nm laser as cooling light to cool rubidium atoms. J.Z. and X.G. performed the experiment. J.Z. wrote the manuscript. Z.X. helped with theoretical analysis. X.G., R.C., and M.H. helped with laser cooling experiment. T.S. and J.C. provided revisions.

The authors declare no competing interests.

DATA AVAILABILITY

Data underlying the results of this study are available from the authors upon request.

[1] R. Ciuryło, E. Tiesinga, S. Kotochigova, and P. S. Julienne, Photoassociation spectroscopy of cold alkaline-earth-metal atoms near the intercombination line, Phys. Rev. A **70**, 062710 (2004).

[2] R. A. Hart, X. Xu, R. Legere, and K. Gibble, A quantum scattering interferometer, Nature (London) **446**, 892 (2007).

[3] A. L. Shaw, P. Scholl, R. Finkelstein, R. B.-S. Tsai, J. Choi, and M. Endres, Erasure cooling, control, and hyperentanglement of motion in optical tweezers, Science **388**, 845 (2025).

[4] D. Wineland, C. Monroe, D. Meekhof, B. King, D. Leibfried, W. Itano, J. Bergquist, D. Berkeland, J. Bollinger, and J. Miller, Quantum state manipulation of trapped atomic ions, Proc. R. Soc. London A **454**, 411 (1998).

[5] S. Chu, L. Hollberg, J. E. Bjorkholm, A. Cable, and A. Ashkin, Three-dimensional viscous confinement and cooling of atoms by resonance radiation pressure, Phys. Rev. Lett. **55**, 48 (1985).

[6] E. L. Raab, M. Prentiss, A. Cable, S. Chu, and D. E. Pritchard, Trapping of neutral sodium atoms with radiation pressure, Phys. Rev. Lett. **59**, 2631 (1987).

[7] H. J. Metcalf and P. Van der Straten, *Laser Cooling and Trapping* (Springer Science & Business Media, New York, 1999).

[8] J. S. Rosenberg, L. Christakis, E. Guardado-Sanchez, Z. Z. Yan, and W. S. Bakr, Observation of the Hanbury Brown–Twiss effect with ultracold molecules, Nat. Phys. **18**, 1062 (2022).

[9] T. Weber, J. Herbig, M. Mark, H.-C. Nagerl, and R. Grimm, Bose-Einstein condensation of cesium, Science **299**, 232 (2003).

[10] X. Zheng, J. Dolde, V. Lochab, B. N. Merriman, H. Li, and S. Kolkowitz, Differential clock comparisons with a multiplexed optical lattice clock, Nature (London) **602**, 425 (2022).

[11] J. Li, X. Chen, D. Zhang, W. Wang, Y. Zhou, M. He, J. Fang, L. Zhou, C. He, J. Jiang, *et al.*, Realization of a cold atom gyroscope in space, Natl. Sci. Rev. **12**, nwaf012 (2025).

[12] A. Aeppli, K. Kim, W. Warfield, M. S. Safronova, and J. Ye, Clock with 8×10^{-19} systematic uncertainty, Phys. Rev. Lett. **133**, 023401 (2024).

[13] T. Zhang, L. Chen, Y. Shu, W. Xu, Y. Cheng, Q. Luo, Z. Hu, and M. Zhou, Ultrahigh-sensitivity Bragg atom gravimeter and its application in testing Lorentz violation, Phys. Rev. Appl. **20**, 014067 (2023).

[14] J. J. Osborne, I. P. McCulloch, B. Yang, P. Hauke, and J. C. Halimeh, Large-scale 2 + 1D U(1) gauge theory with dynamical matter in a cold-atom quantum simulator, Commun. Phys. **8**, 273 (2025).

[15] J. C. Halimeh, M. Aidelsburger, F. Grusdt, P. Hauke, and B. Yang, Cold-atom quantum simulators of gauge theories, Nat. Phys. **21**, 25 (2025).

[16] O. Heavens, Radiative transition probabilities of the lower excited states of the alkali metals, J. Opt. Soc. Am. **51**, 1058 (1961).

[17] C. Gerz, T. Hodapp, P. Jessen, K. Jones, W. Phillips, C. Westbrook, and K. Molmer, The temperature of optical molasses for two different atomic angular momenta, Europhys. Lett. **21**, 661 (1993).

[18] S. Rosi, A. Burchianti, S. Conclave, D. S. Naik, G. Roati, C. Fort, and F. Minardi, λ-enhanced grey molasses on the D_2 transition of rubidium-87 atoms, Sci. Rep. **8**, 1301 (2018).

[19] C. Liang, S. Gao, J. Liu, G. Wang, S. Yan, J. Yang, L. Zhu, and X. Ma, Multi-parameter optimization of polarization gradient cooling for ^{87}Rb atoms based on reinforcement learning, Opt. Express **32**, 40364 (2024).

[20] J. Hu, A. Urvoy, Z. Vendeiro, V. Crépel, W. Chen, and V. Vuletić, Creation of a Bose-condensed gas of ^{87}Rb by laser cooling, Science **358**, 1078 (2017).

[21] A. M. Kaufman, B. J. Lester, and C. A. Regal, Cooling a single atom in an optical tweezer to its quantum ground state, Phys. Rev. X **2**, 041014 (2012).

[22] J. D. Thompson, T. Tiecke, A. S. Zibrov, V. Vuletić, and M. D. Lukin, Coherence and Raman sideband cooling of a single atom in an optical tweezer, Phys. Rev. Lett. **110**, 133001 (2013).

[23] J. Goldwin, S. B. Papp, B. Demarco, and D. S. Jin, Two-species magneto-optical trap with ^{40}K and ^{87}Rb, Phys. Rev. A **65**, 021402(R) (2002).

[24] K. N. Jarvis, J. Devlin, T. Wall, B. Sauer, and M. Tarbutt, Blue-detuned magneto-optical trap, Phys. Rev. Lett. **120**, 083201 (2018).

[25] J. G. Bohnet, Z. Chen, J. M. Weiner, D. Meiser, M. J. Holland, and J. K. Thompson, A steady-state superradiant laser with less than one intracavity photon, Nature (London) **484**, 78 (2012).

[26] H. Xue, Y. Feng, S. Chen, X. Wang, X. Yan, Z. Jiang, and Z. Zhou, A continuous cold atomic beam interferometer, J. Appl. Phys. **117**, 094901 (2015).

[27] R. Gutterres, C. Amiot, A. Fioretti, C. Gabbanini, M. Mazzoni, and O. Dulieu, Determination of the ^{87}Rb $5p$ state dipole matrix element and radiative lifetime from the photoassociation spectroscopy of the $Rb_2 0_g^-(p_{3/2})$ long-range state, Phys. Rev. A **66**, 024502 (2002).

[28] R. C. Das, D. Shylla, A. Bera, and K. Pandey, Narrow-line cooling of ^{87}Rb using $5S_{1/2} \rightarrow 6P_{3/2}$ open transition at 420 nm, J. Phys. B: At. Mol. Opt. Phys. **56**, 025301 (2023).

[29] R. C. Das, T. Ravi, S. Khan, and K. Pandey, Continuous loading of a magneto-optical trap of Rb using a narrow transition, Phys. Rev. A **109**, 063107 (2024).

[30] J. Marek and P. Munster, Radiative lifetimes of excited states of rubidium up to quantum number n = 12, J. Phys. B: At. Mol. Phys. **13**, 1731 (1980).

[31] M. Safronova and U. Safronova, Critically evaluated theoretical energies, lifetimes, hyperfine constants, and multipole polarizabilities in ^{87}Rb, Phys. Rev. A **83**, 052508 (2011).

[32] W. Ketterle, A. Martin, M. A. Joffe, and D. E. Pritchard, Slowing and cooling atoms in isotropic laser light, Phys. Rev. Lett. **69**, 2483 (1992).

[33] H. Batelaan, S. Padua, D. Yang, C. Xie, R. Gupta, and H. Metcalf, Slowing of ^{85}Rb atoms with isotropic light, Phys. Rev. A **49**, 2780 (1994).

[34] J. Wan, X. Wang, X. Zhang, Y. Meng, W. Wang, Y. Sun, and L. Liu, Quasi-one-dimensional diffuse laser cooling of atoms, Phys. Rev. A **105**, 033110 (2022).

[35] X. Wang, Y. Sun, and L. Liu, Realizing fast temperature measurement and simulating Maxwell's demon with nearly nondestructive detection in cold atoms, Photonics Res. **10**, 1947 (2022).

[36] P. Chang, S. Zhang, H. Shang, and J. Chen, Stabilizing diode laser to 1 Hz-level Allan deviation with atomic spectroscopy for Rb four-level active optical frequency standard, Appl. Phys. B **125**, 196 (2019).

[37] J. Zhang, T. Shi, J. Miao, D. Yu, and J. Chen, An extremely bad-cavity laser, npj Quantum Inf. **10**, 87 (2024).

[38] I. I. Ryabtsev, I. I. Beterov, D. B. Tretyakov, V. M. Entin, and E. A. Yakshina, Spectroscopy of cold rubidium Rydberg atoms for applications in quantum information, Phys. Usp. **59**, 196 (2016).

[39] S. Zhang, X. Zhang, J. Tu, Z. Jiang, H. Shang, C. Zhu, W. Yang, J. Cui, and J. Chen, A 420 nm blue diode laser for the

potential rubidium optical frequency standard, Chin. Phys. Lett. **34**, 074211 (2017).

[40] R. Sun, W. Zhao, Y. Zhang, T. Yuan, H. Liu, S. Gu, and J. Chen, 420 nm Rb optical frequency standard with short-term frequency stability below 2×10^{-13}, Opt. Express **34**, 28391 (2026).

[41] S. Zhang, X. Zhang, J. Cui, Z. Jiang, H. Shang, C. Zhu, P. Chang, L. Zhang, J. Tu, and J. Chen, Compact Rb optical frequency standard with 10^{-15} stability, Rev. Sci. Instrum. **88**, 103106 (2017).

[42] L. Salvi, L. Cacciapuoti, G. Tino, and G. Rosi, Atom interferometry with Rb blue transitions, Phys. Rev. Lett. **131**, 103401 (2023).

[43] S. Trémine, E. De Clercq, and P. Verkerk, Isotropic light versus six-beam molasses for Doppler cooling of atoms from background vapor: Theoretical comparison, Phys. Rev. A **96**, 023411 (2017).

[44] X. Guan, J. Zhang, X. Gao, Y. Wang, T. Shi, and J. Chen, A 780 nm optical frequency standard based on diffuse laser cooled ^{87}Rb atoms, Appl. Phys. Lett. **126**, 031104 (2025).

[45] P. Horak, J.-Y. Courtois, and G. Grynberg, Atom cooling and trapping by disorder, Phys. Rev. A **58**, 3953 (1998).

[46] G. Grynberg, P. Horak, and C. Mennerat-Robilliard, Spatial diffusion of atoms cooled in a speckle field, Europhys. Lett. **49**, 424 (2000).

[47] F.-X. Esnault, D. Holleville, N. Rossetto, S. Guerandel, and N. Dimarcq, High-stability compact atomic clock based on isotropic laser cooling, Phys. Rev. A **82**, 033436 (2010).

[48] X. Wang, Y. Sun, H. Cheng, J. Wan, Y. Meng, L. Xiao, and L. Liu, Nearly nondestructive thermometry of labeled cold atoms and application to isotropic laser cooling, Phys. Rev. Appl. **14**, 024030 (2020).

[49] Y. Hsiao, H. Chen, P. Tsai, and Y. Chen, Cold atomic media with ultrahigh optical depths, Phys. Rev. A **90**, 055401 (2014).

[50] S. Sinha, S. Achar, S. Satheesh, and A. Sharma, Precision measurement of the saturation intensity in rubidium at 420 nm, arXiv:2606.30871.

[51] X. Wang, Y. Sun, and L. Liu, Characterization of isotropic laser cooling for application in quantum sensing, Opt. Express **29**, 43435 (2021).